Modeling of solid solution strengthening in FCC alloys: Atomistic simulations, statistical models and elastic continuous approaches

Pierre-Antoine Geslin

Modeling of solid solution strengthening in FCC alloys: atomistic simulations, statistical models and elastic continuous approaches

Pierre-Antoine Geslin[a,*]

[a] *Univ. Lyon, CNRS, INSA Lyon, Université Claude Bernard Lyon 1, MATEIS, UMR5510, 69100 Villeurbanne, France*

Abstract

Solid solution strengthening is a technologically important mechanism controlling the strength of a wide range of alloys. Understanding and predicting the temperature-dependent yield stress of these alloys requires to model the interactions between dislocation and solutes atoms across a wide range of time and length-scales, and therefore necessitates the development of multiple numerical methods (atomistic calculations, statistical approach and continuous elastic models) that are reviewed in this article. The advantages and drawbacks of each methods as well as their complementary character and the connections between them are highlighted.

Introduction

Alloying metals contributes to improve their mechanical properties through different mechanisms [1, 2]. In particular, a large variety of metallic alloys are characterized by large solubility limits over wide temperature ranges, promoting the formation of a single phase where atoms of different species are randomly dispersed in the crystalline lattice. These inhomogeneities form obstacles to dislocation motion, thereby increasing the strength of the alloy, a mechanisms referred to as solid solution strengthening.

This review will focus on the case of substitutional solid solution in face-centered cubic (FCC) alloys, that encompasses a large range of applications of technological importance, such as aluminum alloys of the 1000, 3000 and 5000 series and austenitic stainless steels, respectively used in automotive and nuclear industries [3, 4]. In addition, precipitate-hardened alloys often retain a significant amount of solutes in their matrix phase, therefore taking advantage of both solid solution and precipitate strengthening. This is for instance the case for Ni-based superalloys used in high temperature applications [5, 6]. Furthermore, the recent development of high entropy alloys (HEA) that contain multiple components in comparable quantities largely rely on solid solution strengthening to achieve exceptional mechanical properties [7–11].

Solid solution strengthening in body-cenceted cubic alloys [12, 13] as well as the role of interstitial atoms on strengthening [14], albeit their high interest for numerous applications, are left out of the scope of this review. In addition, we will restrict the discussion to strengthening emerging from immobile solute atoms. At medium to high temperature, the interplay between dislocation glide and solute diffusion can lead to solute drag [15] and dynamical strain ageing [16] that will not be discussed here.

The technological importance of solid solution strengthening in FCC alloys reveals the need for a thorough understanding of the underlying physical mechanisms, and calls for the development of quantitative models able to predict the flow stress of solid-solution alloys as function of compositions and temperature.

In these FCC alloys, the onset of plasticity is controlled by the glide of $\frac{b}{\sqrt{2}}\langle 110\rangle$ dislocations gliding on $\{111\}$ planes. The dislocation core is characterized by a dissociation into into Shockley partials separated by a stacking-fault ribbon [2, 15]. The origins of solid solution strengthening lies in the interactions between solute atoms and dislocations. In particular, it is worth distinguishing different types of interactions. First, the atomic volume of solute atoms are often significantly different than the solvent's, such that they interact with the pressure field around the dislocation [15]. Considering a perfectly straight infinite dislocation, its interaction energy with a solute atom can then be written as function of the position of the solute with respect the dislocation[1]:

*Corresponding authors

[1] throughout this manuscript, we will consider a dislocation ori-

$$E_{int} = -\Delta V p(y_s, z_s) = \frac{\mu b_\perp \Delta V}{3\pi} \frac{1+\nu}{1-\nu} \frac{z_s}{y_s^2 + z_s^2} \quad (1)$$

where ΔV is the volume difference between the solute and solvent atoms and $b_\perp$ denotes the magnitude of the edge Burger's vector of the dislocation. It is interesting to note that this size interaction is effectively long-range since it decreases with the inverse of the distance between the solute and the dislocation.

An other source of interaction is related to the contrast of stiffness between solute and solvent atoms. In a linear elastic framework, this interaction can be expressed as function of the elastic moduli of both components [17, 18]. The corresponding interaction energy decreases with the square of the distance to the dislocation, making it effectively short-range.

An other type of short-range interaction originates from the binding energy of solute atoms with the highly distorted core region of the dislocation or with the stacking fault ribbon between partial dislocations [13, 19, 20].

The interaction between dislocation and solute clusters can also be relevant in non-dilute alloys. In particular, the atomic shear produced by dislocation glide can modify the energy of the system by forming or breaking solute pairs, and the resulting forces can impede dislocation motion [21, 22].

Physically-based modeling tools (atomistic simulations, continuous elastic models, statistical approaches) have been developed to investigate these effects on solid solution strengthening in different systems, in order to predict the yield stress of alloys as function of composition and temperature. The goal of this review is to draw a global picture of solid solution strengthening modeling by describing these different methods and by highlighting their advantages and drawbacks as well as the connections between them.

The first part of this article focuses on atomistic simulations of solute strengthening that provide informative tools to probe the collective influence of solutes on dislocation motion [23]. In section 2, statistical models that rely on various assumptions to average dislocation/solutes interactions are discussed, with a special focus on Labusch-type approaches [24] that have recently been revisited to model accurately both dilute [25] and concentrated solid solution [26]. Section 3 focuses on the development of continuous elastic models that provide a way to overcome time and length-scale limitations of atomistic simulations without relying on the strong assumptions of statistical approaches. Finally, the open questions related to thermally activated glide will be discussed in section 4.

ented along the x direction and gliding in the y direction on the plane of normal z

1. Atomistic simulations

Atomistic simulations appears as a natural tool to investigate interactions between the atomic-scale defects that are solutes atoms and dislocations. It holds the advantage of describing the details of the atomsitic interactions and to naturally incorporate the different types of interactions listed above. The development of accurate interatomic potentials for binary systems and the increase of computational resources in the past decades enabled the use of atomistic calculations to investigate interactions between long dislocations (50-500 nm) and random solid solutions [23].

The strengthening in Al-Mg [27, 28] solid solutions was investigated with embedded atom model (EAM) potentials. Molecular statics simulations [28] can be used to estimate the athermal critical resolved shear stress (CRSS) to make the dislocation glide over a threshold distance. Molecular dynamics simulations can also be used to estimate the dislocation velocity as function of the temperature and applied stress [27]. The results can then be fitted to deduce a temperature-dependent CRSS and the phonon drag coefficient characterizing the dynamic behavior of the dislocation beyond the CRSS [21, 27, 29]. Atomistic results show that both the athermal and temperature-dependent CRSS increase as $c_{Mg}^{2/3}$ with solute content [28], in accordance with Labusch-type models [24] detailed in section 2. It was suggested that strengthening in Al-Mg alloys is dominated by the size difference between solute and solvent atoms. Similar conclusions are reached for Ni-Au alloys [29]. In both alloys, the CRSS of the screw dislocation was found to be approximately half of the edge's, which was rationalized by considering that the pressure field around screw dislocation is weaker than around the edge. In particular, in the case of Ni-Au alloys where the dissociation between partials is significant, solute/partial dislocation interactions can be approximated by Eq. (1): since $b_\perp^{\text{partial edge}}/b_\perp^{\text{part. screw}} = 1/\sqrt{3} = 0.58$, a weaker CRSS is expected for the screw character.

In contrast, Rodary et al. [21] investigated dislocation behavior in Ni-Al alloys and show that the depinning stress scales linearly with the solute concentration. This was attributed to the relatively small size effect in

this system and to the prevalence of strong chemical interactions between Al atoms: the atomic shear produced by partial dislocations forms or breaks Al-Al first neighbors pairs that have a high energy, thereby creating obstacles for dislocation glide. Because both screw and edge dislocations are equally affected, the strengthening was found to have similar magnitude for both characters [30]. A statistical model was also developed to take into account this strengthening of chemical nature [22, 30].

More recently, atomistic simulations were used to investigate solute strengthening in various FCC multi-component concentrated alloys [31–33]. The CRSS for the screw dislocation was found to be smaller than the edge's [31, 34], revealing the prevalence of elastic interactions. In addition, the fluctuations of the stacking fault energy with the local composition was evidenced and suggested to contribute significantly to strengthening [32, 33, 35–39].

The high degree of roughening of the dislocation line was also highlighted in several studies [31–34, 39, 40]. In particular, the roughness of the dislocation was precisely quantified as function of temperature and applied stress in a FeNiCr austenitic steel [40], and it was showed that at the CRSS, the line is self-afine and is characterized by a roughness exponent $0.6 < \alpha < 0.8$. Similar conclusions were reached by Patinet who found $\alpha = 0.85 \pm 0.05$ in the vicinity of the CRSS of a edge dislocation gliding in a binary Ni-Al alloy [41].

Atomistic calculations also opens the possibility to investigate the role of short-range order (SRO) in random alloys [29, 42, 43]: Monte-Carlo simulations can be used to equilibrate the atomic configuration at a given temperature by minimizing its free energy. Such relaxation can promote the formation of atomic bounds of lower energy, driving the system away from a purely random configuration by introducing order. In several systems, SRO has been shown to contribute to strengthening by increasing the CRSS [42, 44]. This strengthening is qualitatively explained by the atomic slip produced by the dislocation glide that breaks the SRO, forming a band of higher energy in the dislocation glide plane. The resulting force impedes dislocation motion.

Atomistic calculations can therefore be an informative tool to decipher the interactions between dislocations and solid solutions. However, it was recognized very early that they bears some limitations and cannot reveal the full picture of solid solution strengthening [23]. First, the computed critical stress depends strongly on both the dislocation length and the gliding distance [34, 45]. Second, molecular dynamics simulations remains very limited in terms of time-scales. Unless prohibitive computational resources are used [46], atomistic simulations are restricted to ns to μs time-scales. The thermally activated events probed at these short time-scales can be significantly different from the ones controlling the flow stress on experimental times.

Lastly, atomistic simulations rely on the development of accurate interatomic potentials. EAM and modified-EAM formalisms offer physically-based frameworks to model atomic interactions for a large variety of systems [47–49]. While these potentials hold the advantage of being computationally cheap, they often suffer from a lack of accuracy [50]. To overcome this difficulty, other formalisms have been developed: in particular, Machine-Learning potentials based on artificial intelligence methods [51, 52] can achieve a much better accuracy. However, these potentials are also more computationally expensive than EAM and modified-EAM formalisms, revealing a trade-off between the accuracy of the potential and the accessible length and time scales [50, 53]. Moreover, this type of potentials are trained using a data-base of atomic configuration and the transferability of a potential to describe configurations outside of the training data can be limited [52, 54].

Even if the recent development of Machine-Learning potentials for various systems offer more accurate descriptions of atomic interactions, atomistic simulations operate at small length and time scales and may not reveal the full picture of the mechanisms controlling solute strengthening in experimental conditions. These limitations reveal the need for an upscaling approach, trough the development of quantitative statistical models (section 2) or higher-scale continuous framework enabling to operate at greater time and length-scales than atomistic calculations (section 3).

2. Statistical treatments and energy-based models

The limitations of atomistic simulations encourage to consider dislocation glide in random alloys as a statistical problem to estimate the flow stress of alloys. Several statistical approaches have been developed through the years [24, 55–60] and detailed descriptions of these historical approaches can be found elsewhere [1, 13, 30]. In the following, we will recall the important distinction between individual and collective pinning before focusing on the recent developments of Labusch-type approaches [24–26] and on their application to specific systems.

2.1. Statistical models for individual pinning

Individual pinning refers to a description of solid solution strengthening where the dislocation is assumed

to bow-out between solutes modeled as strong point-like obstacles. Friedel [60] and Fleischer [55] proposed statistical models of this situation where the flow stress of an alloy of solute concentration c is expressed as function of the dislocation line-tension Γ, the obstacle strength f_0 and the average distance between obstacles in the glide plane, eventually yielding the following scaling for the athermal CRSS [13, 55, 60]:

$$\tau_{c,0} \sim \frac{f_0^{3/2}\sqrt{c}}{\sqrt{\Gamma}}. \quad (2)$$

However, the dislocation/solute interaction includes a long-range elastic component emerging from the size interaction embedded in Eq. (1) such that describing solutes as point-like obstacles can only remain valid for systems dominated by short-range dislocation/solute interactions or in very dilute alloys [61].

2.2. *Statistical model for collective pinning*

In contrast, collective pinning (also known as weak pinning) approaches consider that strengthening originates from fluctuations of the collective force attributed to an ensemble of solutes along the dislocation line [24, 57–60, 62]. Because of the randomness of the alloy, this collective pinning force is either positive or negative, therefore pushing or pulling the dislocation in environments of lower energies. Thus, the dislocation is assumed to adopt a wavy zig-zag shape (see Fig. 1.a) where segment of characteristic lengths ζ glide a distance w. These quantities are determined by the balance between solute-dislocation interactions and the line-tension force. To keep calculations tractable, two assumptions were made by Labusch in Ref. [24]: (i) the solutes outside the dislocation glide plane were neglected and (ii) the dislocation/solute interactions were considered to have a finite range and a maximum strength f_0. After determining the characteristic length ζ, the CRSS at 0 K is determined as the stress required to overcome the collective solute force on a dislocation segment ζ, eventually yielding:

$$\tau_{c,0} \sim \frac{c^{2/3} f_0^{4/3}}{\Gamma^{1/3}} \quad (3)$$

These historical models rely on the assumption that solutes exert a given maximum force on the dislocation, while solutes located on different planes are characterized by different forces. Including obstacles of various strengths is possible but at the expense of the analytical tractability of the mathematical treatment [30, 56]. Moreover, considering finite-range interactions between dislocations and solutes conflicts with the long-range nature of the size interactions.

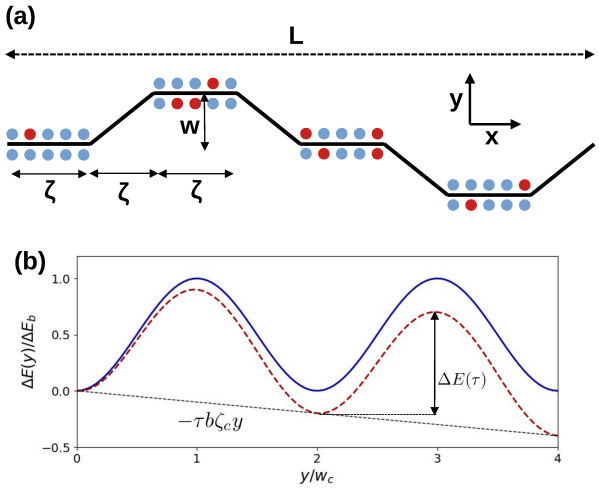

Figure 1: (a) Dislocation line adopting a zig-zag shape with characteristic segment length ζ and amplitude w [13, 25, 26]. (b) Energy profile assumed for a segment of length ζ_c at zero applied stress (blue continuous line) and with applied stress (red dashed line)

These issues can be resolved by switching points of view: instead of considering obstacles of various strengths, Zaiser considered the fluctuation of interaction energies between a dislocation and an ensemble of solutes [63]. This strategy was later taken over by Leyson and Curtin [25] to develop a quantitative theory of strengthening that is described in the following.

We first introduce the characteristic change of energy per atomic plane perpendicular to the dislocation line, upon a displacement w of a straight dislocation in the glide direction:

$$\Delta\tilde{E}_p(w) = \left[c\sum_i \left(U(y_i - w, z_i) - U(y_i, z_i)\right)^2\right]^{1/2}, \quad (4)$$

where $U(y_i, z_i)$ is the interaction energy between a solute atom located at position (y_i, z_i) with respect to the dislocation line and where the sum runs over all the lattice sites of the crystallographic plane perpendicular to the dislocation line.

Considering that along a dislocation of length L, segments of length ζ move backward or forward over a distance w to more favorable positions (see Fig. 1.a), the total energy change of the system is given by

$$\Delta E_{tot}(\zeta, w) = \left[\frac{\Gamma w^2}{2\zeta} - \sqrt{\frac{\zeta}{\sqrt{3}b}}\Delta\tilde{E}_p(w)\right]\frac{L}{2\zeta}, \quad (5)$$

where the first term is related to the line-energy cost of the bow-out and the second term is the typical energy

gain related to the motion of the dislocation segment into a more favorable position. The numerical factor $\zeta/\sqrt{3}b$ is the number of atomic planes perpendicular to the dislocation segment of length ζ for a FCC crystal.

Minimizing $\Delta E_{tot}(\zeta, w)$ with respect to ζ and w yields characteristic quantities ζ_c and w_c describing the dislocation zig-zag shape. In particular, this minimization yields

$$\zeta_c(w) = \left(4\sqrt{3} \frac{\Gamma^2 w^4 b}{\Delta \tilde{E}_p^2(w)} \right)^{1/3}. \quad (6)$$

To obtain a CRSS from Eq. (5), it is then assumed that the dislocation segment of length ζ_c experiences a periodic energy profiles of period $2w_c$ (the characteristic distance between a minimum and a maximum of energy being w_c) and of characteristic energy barrier ΔE_b (see Fig. 1.b) that is expressed as function of Γ and $\Delta \tilde{E}_p(w_c)$.

An applied stress tilts this energy profile, and it is straightforward to express the athermal stress to unpin the dislocation [25]:

$$\tau_{c,0} = 1.01 \left(\frac{\Delta \tilde{E}_p(w_c)^4}{\Gamma b^5 w_c^5} \right)^{1/3}. \quad (7)$$

Since $\Delta \tilde{E}_p(w_c) \sim \sqrt{c}$, the same power dependence $\tau_c \sim c^{2/3}$ as in the historical Labusch approach (Eq. (3)) is recovered.

At $\tau < \tau_{c,0}$, glide occurs through thermal activation. The simplest description of this regime consists in considering that the limiting mechanism is the movement of a dislocation segment of length ζ_c over the characteristic energy barrier represented in Fig. 1.b. At $\tau < \tau_y^0$, the activation energy decreases with τ as:

$$\Delta E(\tau) = \Delta E_b \left(1 - \frac{\tau_c}{\tau} \right)^{3/2}, \quad (8)$$

and the dislocation average velocity is obtained from a simple Arrhenius relation. We can then deduce the CRSS as function of strain rate $\dot{\varepsilon}$ and temperature T [13, 25]:

$$\tau_c(T, \dot{\varepsilon}) = \tau_c^0 \left[1 - \left(\frac{k_b T}{\Delta E_b} \ln(\dot{\varepsilon_0}/\dot{\varepsilon}) \right)^{2/3} \right] \quad (9)$$

where $\dot{\varepsilon_0}$ is a reference strain rate estimated at $\dot{\varepsilon_0} = 10^5 s^{-1}$ [13]. The limitations of this treatment of thermally activated glide are discussed in section 4.

Applying this Labusch-type model to concentrated systems and high entropy alloys (HEAs) appeared highly desirable but also challenging because the distinction between solute and solvent break down in these multi-component concentrated alloys. Some authors [64, 65] attempted to model the strength of HEAs by considering the influence of each species on strengthening before averaging their contribution in a generalized Labusch model.

A more physically-based treatment was proposed by Varvenne et al. in Ref. [26], where the energy-based Labusch model described above was successfully generalized to incorporate the role of several species by replacing Eq. (4) by:

$$\Delta \tilde{E}_p(w) = \left[\sum_n c_n \sum_i \left(U_n(y_i - w, z_i) - U_n(y_i, z_i) \right)^2 \right]^{1/2} \quad (10)$$

where the first sum runs over the different components of the alloy. As originally suggested in Ref. [26], the interaction energies $U_n(y_i - w, z_i)$ are not unique for concentrated alloys because they depend on the local chemical environment surrounding the solute n. The fluctuations of this quantity can also be incorporated in the formalism [26]

This strengthening model for concentrated alloys was further extended to incorporate the role of short-range chemical interactions between solutes [66] that controls strengthening in Ni-Al alloys [66, 67].

2.3. *Parametrization and predictions of Labusch-type models*

This type of energy-based Labusch model holds the advantage of relying only on a few parameters: the interaction energies $U_n(y_i, z_i)$ between a straight dislocation line and a solute atom n located on the site (y_i, z_i) and the line-tension coefficient Γ. In the following, we distinguish different parameterization strategies for dilute and concentrated alloys and discuss their prediction capabilities.

2.3.1. *Dilute alloys*

The line-tension coefficient is often estimated as $\Gamma \simeq \alpha \mu b^2$, where α typically ranges between 0.05 and 0.2 [15]. In the case of a dilute alloy, atomistic calculations can be used to estimate precisely the line tension parameter of the solvent, either at $0K$ using molecular statics [68–70] or in temperature using molecular dynamics [71, 72].

In the case of dilute alloys, the pure solvent matrix can be considered as the reference frame and ab-initio calculations can be performed to compute the interaction energies $U(y_i, z_i)$ between the dislocation and solute atoms located at different positions [25]. Such finely parameterized model can predict the magnitude

of solid solution strengthening in dilute alloys and quantitative comparison with experimental measurements in Al alloys have been achieved for both the temperature-dependent yield-stress [25, 73] and the activation volume [13].

To compute the interaction energies $U(y_i, z_i)$, Ma et al. [74] used a different strategy by considering the interactions between a solute atom and a Peierls-Nabarro description of the dislocation [75] and by distinguishing between volumetric and slip misfit interaction energies. While such approach is computationally efficient because it does not rely on a large number of ab-initio calculations, its prediction are in quantitative agreement with experimental measurements of the temperature-dependent yield stress of dilute Al-Li and Al-Mg alloys [74].

2.3.2. *Concentrated alloys*

For concentrated alloys, the distinction between solute and solvent breaks down, making it less straightforward to estimate the activation energies $U_n(y_i, z_i)$. This quantity can be computed by considering that the appropriate reference system is an average medium holding the same properties (lattice constant, elastic moduli, stacking-fault energy, ...) as the concentrated alloy. Varvenne and coworkers showed that EAM potentials describing the interactions between species in an alloy can be averaged to obtain an interatomic potential for the average atom [76]. This average atom potential reproduces accurately the properties of concentrated alloys [76], and opens the possibility to compute average interaction energies $U_n(y_i, z_i)$ by considering a solute embedded into a matrix of average atoms. This average atom potential can also be used to estimate the effective line-tension coefficient Γ of the concentrated alloy as done in Ref. [26] . Using these atomistically determined parameters, Varvenne et al. successfully reproduce the composition-dependent yield stress of FeNiCr alloys [26]. Such average-atom model can be derived for some interatomic potentials (i.e. pair potentials and EAM) but applying this strategy to other potential formalisms (in particular for machine-learning potentials) appears challenging because of the necessity to adopt an averaging procedure adapted to the potential formalism.

An other strategy consists in considering that the size effect dominates the dislocation/solute interactions such that $U_n(x_i, y_i)$ can be estimated from the pressure field around the dislocation (e.g. Eq. (1)). The misfit volume of the species is computed with respect to the average atomic volume of the alloy taken as reference [26]. Such simplification leads to compact expressions for the athermal CRSS (Eq. (7)) and the characteristic energy barrier (Eq. (8)) that become functions of the elastic moduli μ and ν of the alloy and the misfit volumes of species ΔV_n. These quantities can be obtained from atomistic calculations: the use of Special Quasi-random Structures (SQS) [77] allows to estimate these quantities from small simulation cells compatible with ab-initio calculations [78–81].

An additional simplification consists in considering that the lattice spacing and the elastic moduli of the alloy depend linearly on the composition. Employing these rules of mixture allows for an efficient screening of the large compositional space of FCC concentrated alloys valuable for alloy design purposes [82, 83]. However, the atomic volumes of elements Fe, Ni, Cr, Mn and Co are rather similar (they deviate from one another by a few percents at most), such that strengthening is these alloy may not be entirely controlled by the size effect; in this situation, the use of an elastic formulation parameterized with rules of mixture can be hazardous. Coury et al. [83] showed that the atomic radii of each species have to be carefully chosen to reproduce experimentally measured yield stresses in FeNiCrMnCo alloys. On the other hand, the influence of other addition elements in FeNiCrMnCo alloys is well captured by the elastic formulation of the model: the atomic size of Al [84], Pd [85] and V [86] are significantly larger than Fe, Ni, Cr, Mn and Co, such that the elastic model reproduces well the increase of yield stress measured experimentally upon their addition.

The elastic formulation of the model was also applied to noble metals high entropy alloys, with parameters obtained with rules of mixture [87] and from DFT calculations [80]. Even though a good agreement was achieved with a few experimental measurements, more recent experimental measurements across the compositional space of AuCuNiPdPt alloys evidenced discrepancies with the prediction of the elastic model [88, 89], possibly revealing the limitations of the elastic formulation to describe this class of alloys.

Some authors highlighted the difficulties to parameterize the model to reach quantitative predictions for concentrated FCC alloys [90, 91]: indeed, going beyond the elastic approximation requires to develop an average atom potential that depends on the alloy composition. As an alternative, Huang et al. [91] suggested to modify the physically-based elastic model of Varvenne et al. [26] to incorporate the influence of additional descriptors (such as the charge transfer between elements) in addition to the size effect. The authors used a machine learning method to determine which descriptors to add into the formulation and how to incorporate them, eventually yielding good agreement with experimental mea-

surements.

The recent formulation of the Labusch-type approaches therefore provide a theoretical framework to model strengthening in both dilute and concentrated solid solution. Quantitative comparisons with experimental results can be achieved if the parameters are carefully obtained from atomistic calculations [25, 26, 73]. The simplified elastic formulation of the model has also been shown to yield good agreement with experiments if strengthening is dominated by size effects. However, the assumptions necessary to derive the model can be highlighted: first, the critical stress to unpin the dislocation is predicted by considering a single characteristic length, while atomistic calculations clearly show that the elastic line is rough over all length-scales at the depinning threshold [40, 41]. Moreover, considering than the CRSS is derived from the characteristic energy $\Delta\tilde{E}_p$ might seem counter-intuitive because unpinning occurs when the strongest pinning configuration is overcame, which might be controlled by extreme value statistics. Finally, simplifying the energy landscape experienced by the dislocation by a 1D periodic profile (see Fig. 1.b) can seem simplistic and could neglect important features of the dislocation/solute interactions.

3. Elastic continuous models

Because of the limitations of atomistic simulations and the strong assumptions necessary to derive the statistical models, it seems desirable to develop continuous models of dislocation depinning that go beyond the atomic size and time-scales while incorporating the behavior of the dislocation over all wave-lengths. In contrast with atomistic calculations, such approaches also allow to incorporate the role of different ingredients (size effect interactions, short-range chemical interactions, line-tension approximation, long-range elasticity, etc.) in a well-controlled way in order to to better test their influence. In addition, such well-controlled continuous model can contribute to better justify the assumptions of the statistical model, thereby reinforcing the theoretical foundation of these approaches.

The different approaches discussed in this section rely on a simplified description of the dislocation as a function $h(x)$ (x denoting the line direction). The movement of the elastic line impeded by a quenched disorder can be modeled by:

$$B\frac{\partial h}{\partial t} = -\Gamma\frac{\partial^2 h}{\partial x^2} + f(x, h(x)) + f_a \qquad (11)$$

where B is a kinetic parameter, Γ is the line-tension coefficient, and $f(x, h(x))$ denotes the quenched random force impeding the line motion, and f_a is the force applied to the system (i.e. the resolved shear stress in the case of dislocations).

The depinning transition occurs at a critical stress f_c where the applied force overcomes the random force impeding dislocation motion: (i) for $f_a < f_c$, the dislocation line curves in the random environment and find local forces that balance out the applied force f_a. (ii) For $f_a > f_c$, the applied force is large enough to prevent the line from finding an equilibrium position and the line glides freely. (iii) In the limit $f_a \gg f_c$, the applied force becomes large compared to the random forces and the line-tension term, and the line reach a constant velocity $v = f_a/B$.

3.1. Choice of the random force field

In such framework, a continuous elastic model was proposed by Foreman and Makin [92] that investigated the glide of an elastic line through a field of randomly located point-like obstacles. In this situation, the random force $f(x, y)$ is non-zero only on random locations in the glide plane. This numerical model corresponds to the individual pinning situation of the Fleischer-Friedel models [55, 60] and the numerical results where found to agree with the prediction of the statistical treatment [92].

In the conext of collective pinning, Arsenault et al. [93, 94] built a random noise environment $f(x, y)$ corresponding to the stresses of misfitting solutes randomly placed in the vicinity of the dislocation. Going byound this elastic description, the forces of individual pinning sites can be determined from atomistic simulations [45] and a random force field $f(x, y)$ can be built by summing the contributions of randomly located obstacles [45, 95]. This type of atomistically-informed elastic model was shown to reproduce accurately the CRSS obtained from atomistic simulations of Al-Mg and Ni-Al alloys [45].

However, it seems challenging to apply this type of approach to multi-component concentrated alloys because characterizing and incorporating in a self-consistent way the interactions with all possible atomic arrangement appears as a formidable task. In this context, it seems more suitable to describe the force $f(x, y)$ as a random field: for example, Zhai and Zaiser [96] investigated dislocation depinning in a quenched disorder chosen to be uncorrelated along the direction of the dislocation line and with short-range correlations in the propagation direction.

To relate the statistical properties of the random field $f(x, y)$ (variance and spatial correlations) to the alloy properties (composition, elastic moduli,...), Geslin et al. proposed a microelasticity model of random alloys

[97, 98] that is briefly summarized in the following. Each atom type n is described as a spherical dilatational inclusion of eigenstrain ε_n, a quantity that is directly proportional to the misfit volume ΔV_n entering the statistical models discussed in section 2. These inclusions are randomly located on the crystalline lattice. Using the stress field around such inclusion [18] and making use of the superposition principle, the shear stress at a given point of the lattice can be expressed as the sum of all stresses emerging from the surrounding inclusions. As shown in Ref. [97], this random number follows a Gaussian distribution of variance

$$\langle \tau_p^2 \rangle = A\mu^2 \left(\frac{1+\nu}{1-\nu} \right)^2 \Delta\varepsilon^2 \tag{12}$$

where A is a geometric prefactor that depends on the lattice (FCC or BCC) and $\Delta\varepsilon^2 = \sum_n c_n \varepsilon_n^2$ is the variance of atomic eigenstrain. As for statistical models (see section 2), elastic parameters μ, ν and $\Delta\varepsilon^2$ can be calculated from atomistic simulations using EAM potential as in Ref. [97] or ab-initio SQS cells. In addition, atomistic calculations can also yield an estimate of $\langle \tau_p^2 \rangle$ by computing the virial atomic stress, and the prediction of Eq. (12) has been shown to compare well with atomistic results in the case of Al-Mg alloys [97].

Furthermore, this elastic framework can be used to obtain the spatial correlations of the stress field associated with a random alloy [98]. In order to keep the calculations tractable analytically, the eigenstrains are spatially spread out around their lattice site with a Gaussian shape-function of standard deviation a (in practice, $a \simeq 1$Å).

The spatial correlations of a given shear stress component, say τ_{ij}, are shown to be highly anisotropic (see Fig. 3.1). Along the transverse direction $k \neq i, j$, the spatial correlations denoted $\Sigma_T(d)$ are positive and decrease as $1/d^3$ (red continuous curve on Fig. 3.1). On the other hand, in the longitudinal directions i and j, the correlations $\Sigma_L(d)$ are positive at short range and negative at long range (blue dashed curved in Fig. 3.1). Interestingly, both $\Sigma_T(d)$ and $\Sigma_L(d)$ die out as $1/d^3$, which has been demonstrated as a general property of stress correlations in random elastic media [99]. Combining these spatial correlations, it is also possible to obtain the stress correlations in a plane as shown on the inset of Fig. 3.1.

Let us consider a glide plane of normal z and a dislocation lying along the x direction having a Burger vector $b = (b_x, b_y)$. The Peach-Khoeler force acting on the dislocation in the propagation direction y is given by $f(x, y) = b_x \tau_{xz}(x, y) + b_y \tau_{yz}(x, y)$. Therefore, a pure edge

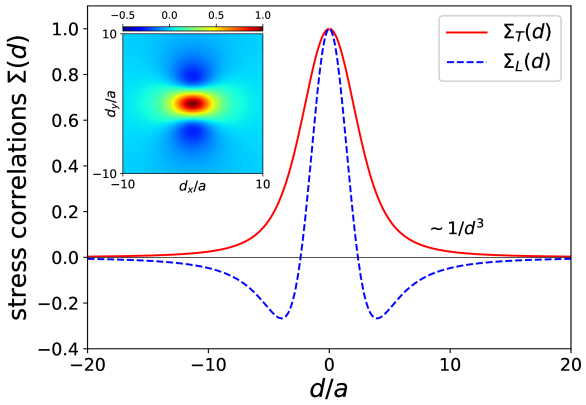

Figure 2: Spatial correlations of a shear stress along the transverse (red line) and longitudinal (dashed blue) directions (see text). The inset shows the interplay of these correlations in 2D.

character will be only sensitive to the stress $\tau_{yz}(x, y)$ that displays positive correlations along the line direction x and negative correlations along the propagation direction (see inset of Fig. 3.1), while the stress correlations acting on the screw character are reversed: negative along the line direction and positive in the propagation direction. We note that the force field for mixed dislocations is not simply the sum of independent stress fields, because $\tau_{xz}(x, y)$ and $\tau_{yz}(x, y)$ are correlated.

Rida et al. [100] developed a numerical dislocation dynamics model based on a spectral solver to find efficiently the equilibrium configuration of the dislocation at a given stress. Increasing incrementally the applied stress until no equilibrium configuration can be found enabled to estimate the athermal CRSS of both edge and screw dislocations evolving in correlated environment. The simulations results reported in Fig. 3 showed that the CRSS of the screw dislocation is significantly smaller than for the edge, which is a direct consequence of the different stress correlations they experience.

3.2. *Statistical models and links with Labusch-type approaches*

Scaling arguments originally attributed to Larkin [101] can be used to estimate the critical force to unpin an elastic line as function of the statistical properties (variance and spatial correlations) of the random field [96, 102, 103]. We consider the case of a random field f having correlations of range w in the propagation direction. Considering a line segment of length λ assumed to remain straight, the pinning force acting on this segment is a random variable and its characteristic magnitude can be approximated by:

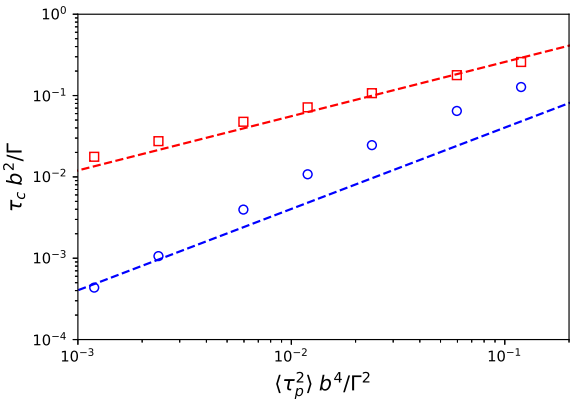

Figure 3: Athermal CRSS determined numerically (symbols) for pure edge and screw dislocations. Dashed lines are prediction of a statistical model Eqs. (15-16).

$$f_p = \left[\int_0^\lambda \int_0^\lambda \langle f(x,y) f(x',y)\rangle dx dx'\right]^{1/2}. \tag{13}$$

Under the influence of this force, the line forms a bulge of characteristic amplitude w. Assuming equilibrium and equating the line-tension force of such bow-out with f_p reveals a characteristic length of the problem, usually referred as Larkin length. As an example, in the case of uncorrelated forces along the line, $f_p \sim \sqrt{\lambda \langle f^2\rangle}$ and

$$\lambda_L \sim \left(\frac{\Gamma w}{\sqrt{\langle f^2\rangle}}\right)^{2/3} \tag{14}$$

For small segments of length $\lambda \ll \lambda_L$, the line-tension dominates over the pinning force f_p and the line does not bow out beyond w. On lengths $\lambda \gg \lambda_L$, this line-tension becomes small compared to the pinning force: the elastic line bows-out on lengths greater than w and explores more favorable configurations in the random field.

As pointed out previously [63, 96], Larkin's length is equivalent to the characteristic length-scale ζ_c of Labusch-type approaches (see section 2) that is also derived as a balance between line-tension and solute interactions contributions.

Similarly to the Labusch-type models, the central assumption is to consider that the depinning transition is controlled by the unpinning of segment lengths λ_L. Equating the pinning force f_p with the applied force acting on the segment length λ_L yields an estimate of critical force to unpin the line. This reasoning has been applied to the case of dislocations evolving in correlated force field [100] and yields different scaling laws for the CRSS of edge and screw dislocations:

$$\tau_{c,0}^{edge} = \left(\frac{15a}{4\sqrt{2}}\right)^{2/3} \left(\frac{b}{\Gamma w_e}\right)^{1/3} \langle\tau_p^2\rangle^{2/3} \tag{15}$$

$$\tau_{c,0}^{screw} = \frac{10a^2 b}{\Gamma \pi w_s} \langle\tau_p^2\rangle \tag{16}$$

where w_s and w_e denote the correlation lengths in the propagation direction that are different for the edge and screw characters. These theoretical estimates are shown with dash lines on Fig. 3.

For the edge case, we recover the well-established scaling $\tau_c^{edge} \sim \langle\tau_p^2\rangle^{2/3}$ [96, 102, 103]. Also, by considering that the variance of the pinning shear stress is given by Eq. (12), we obtain the following scaling between the CRSS and the properties of the alloy (composition, elastic moduli and line tension):

$$\tau_{c,0}^{edge} \sim \frac{\mu^{4/3}}{\Gamma^{1/3}} \left(\frac{1+\nu}{1-\nu}\right)^{4/3} \left(\sum_n c_n \Delta\varepsilon_n^2\right)^{2/3}, \tag{17}$$

which is identical to the scaling derived by Varvenne et al. in the elastic formulation of their model [26, 84, 87].

The situation is however different for the screw dislocation where Larkin's approach yields a linear scaling between $\tau_c \sim \langle\tau_p^2\rangle$, as a consequence of the negative stress correlations along the dislocation line. As shown in Fig. 3, this scaling does not match well the numerical results that shows a steeper increase of τ_c with $\langle\tau_p^2\rangle$ at low stresses. This discrepancy remains to be clarified even if the situation of an isolated dislocation of pure screw character remains idealized because of the dissociation into partials in FCC alloys [15].

It is valuable to discuss the connection between Larkin's approach and energy-based models presented in section 2. In particular, force-based models assume that the segments bow out over an amplitude w (related to the correlations of the random field), while the value of w results from the minimization of Eq. 5 in energy-based models. A connection between both approaches have been proposed in Ref. [100], where the change of energy upon dislocation glide $\Delta\tilde{E}_p(w)$ is related to the work of the random pinning force. For the edge dislocation, this comparison reveals that both models yield very comparable estimates for the CRSS that are consistent with numerical results shown in Fig. 3. This agreement reinforces the validity of the assumptions used in statistical models and suggests that the athermal CRSS can be estimated based on a characteristic length-scale even though the dislocation is rough over all length-scales.

Energy-based models are however not applicable to the pure screw dislocation because the interaction energy between a dilatationnal solute and a straight screw dislocation is nil. The non-zero CRSS reported in Fig. 3 for the screw dislocation results from the roughening of the dislocation away from a straight line.

Furthermore, it was attempted to apply a similar statistical treatment to mixed dislocations [104] and dissociated dislocations [105]. Mixed dislocations are sensitive to both stress fields τ_{xz} and τ_{yz}; while the authors of Refs. [104, 105] used the spatial correlations of τ_{xz} and τ_{yz} shown in Fig. 3.1, the non-zero cross-correlations between these components was however not considered.

3.3. role of long-range elasticity

Continuous elastic models can also be used to check if the line-tension approximation is suitable to model dislocation pinning. Indeed, dislocations self-energy is characterized by long-range elastic interactions, such that the dislocation gets logarithmically stiffer on longer wavelengths [15, 71]. In the contexts of forest hardening and solid solution hardening, it was shown that incorporating these long-range elastic effects do not modify significantly the dislocation behavior [96, 103]. Similar conclusions was reached in Ref. [100] where long-range elastic interactions can be incorporated without additional numerical cost in the Fourier-based solver. In particular, the dependence of the CRSS on the variance of the pinning field displays the same features as in Fig. 3 if long-range elasticity is accounted for.

4. Thermally activated glide

For applied stress below the CRSS, i.e. $\tau < \tau_c$, the dislocation moves through thermally activated events. In their original formulations [25, 26, 84], energy-based Labusch models assume that this regime can be described by the thermally activated glide of segment of length ζ_c (see Eqs. (8-9)).

However, it was demonstrated theoretically [63, 106] that the characteristic size of thermally activated events increases for decreasing applied stresses. This behavior is also consistent with experimental observations showing that the activation volume of thermally activated glide decreases for stronger applied stresses [107–109].

The increase of the size of thermally activated events is related to an increase of their activation energy: while Labusch suggested that the activation energy of these events diverges logarithmically with decreasing stresses [106], Zaiser used scaling arguments to show that the divergence follows a power-law [63]:

$$\Delta E(\tau) \sim (\tau_{c,0}/\tau)^{\mu}, \tag{18}$$

with an exponent μ that depends on the roughness exponent α of the dislocation line through the relation:

$$\mu = \frac{2\alpha - 1}{2 - \alpha}. \tag{19}$$

Leyson and Curtin [110] extended their Labusch-type approach by considering multiple hierarchical bow-outs. By minimizing the energy of the hierarchical configuration, they show that the bow-out lengths and amplitudes are consistent with a roughness exponent $\alpha \simeq 2/3$, which is in accordance with results obtained from atomistic calculations [40, 41]. However, it was found that the activation energy at low stress increases with a power law of exponent $\mu \simeq 0.54$, which does not satisfy Eq. (19). Nevertheless, this new description of the thermally activated events shows satisfactory agreement with experimental measurements of the temperature-dependent yield stress and activation volumes for various dilute copper alloys [110].

Thermal activation has also been extensively studied in the larger framework of the depinning of an elastic line in a random field [102, 111–113], where similar scaling arguments were used to reach Eqs. (18-19) [113, 114]. While stochastic Langevin dynamics allows to explore the influence of thermal activation at moderate applied forces [115], the limit of small forces remains out of reach because of the divergence of the activation energies between metastable states.

The development of efficient algorithms allowed to investigate this limit by enumerating the successive thermally activated events [116, 117]. These numerical results allowed to clarify the validity of Eqs. (18-19). Moreover, they shed light on the complexity of thermally activated glide: in the limit of vanishing force and temperature, the size of thermally activated events follow a scale-free power-law distribution and the thermally activated events appear to be spatially and temporally correlated [117].

5. Conclusion and outlook

The complementary modelling approaches reviewed in this manuscript enable to investigate solid solution strengthening on different size and length-scales. It was shown that molecular dynamics simulations can be used as an informative tool to investigate the collective effect of a ensemble of solutes on a dislocation. In particular, it allows to distinguish if dislocation/solute interactions

is dominated by size effects (as in the model Al-Mg system) [27, 28], solute-solute interactions (as in Ni-Al) [21, 30, 45] or by the fluctuations of the stacking fault energy [37, 38]. To overcome size and length-scale limitations of atomistic simulations, two paths can be followed: the development of statistical models or multiscale numerical approaches.

Section 2 demonstrates the success of recently developed energy-based Labsuch statistical approaches to predict experimental yield stress of dilute and concentrated alloys [25, 26, 84]. The underlying assumption is that the athermal CRSS is controlled by a unique length-scale emerging from the balance between the dislocation line-tension and the strength of solute/dislocation interactions. The parameters entering the model can be determined from atomistic calculations (either with ab-initio or classical potentials), providing quantitative predictions of yield stress without adjustable parameters. If the size effect is assumed to dominate strengthening, an elastic formulation of the model can also be used. However, such simplification can be hazardous if the atomic size mismatch between the species of the alloy is small.

Another upscaling strategy consists in developing meso-scale continuous models of a dislocation line gliding in a random force field that reproduces the statistical properties of the stress field emerging from randomly located solutes. This was realized for solutes of different sizes that interact elastically with the dislocation [97, 98]. Despite the fact that the dislocation becomes rough on all length-scales at the depinning transition, it was shown that a statistical model relying on a single length-scale agrees well with numerical results for the relevant case of an edge dislocation [100]. Such agreement also reveals that energy-based theories and force-based models are consistent, thereby reinforcing the theoretical ground on which the statistical models are built.

The picture is however less clear for thermally activated glide. While both Labusch-type approaches [110] and force-based models [116] reveal the necessity to incorporate multiple length-scales to capture thermally activated glide below the athermal CRSS, both approaches disagree on the exponent of the power-law divergence of the activation energy away from the depinning threshold. This difference reveals that further theoretical and numerical investigations are necessary to clarify the physics of thermally activated glide, and better justify the assumptions commonly made in energy-based statistical approaches [110]. The recent application of the nudged elastic band to dislocations glide [118–120] and the clarification of thermal fluctuations of dislocations [71, 72, 118] are laying the groundwork for such investigations. It would also be valuable to take profit of the numerical methods developed in the larger framework of depinning of elastic line [113], by applying them to the case of dislocation glide and investigating the influence of the correlated force field characterised in Ref. [97, 98]. Also, because multiple length-scales are involved in thermally activated glide, it would also be valuable to investigate carefully the influence of long-range elasticity that stiffen the dislocation line-tension on longer length-scales.

The meso-scale elastic models described in section 3 could also be extended to incorporate effects beyond the elastic interactions between solutes and a compact dislocation line [100]; in particular, it seems essential to incorporate the dissociation of dislocation into partials characteristic of most FCC alloys. Furthermore, it also appears valuable to investigate how the random stress field is altered by the influence elastic anisotropy, short-range order and environment-dependent elastic interactions beyond the size effect [121]. Finally, it was shown that the strength of concentrated alloys can be largely influenced by the fluctuation of stacking fault energy [37, 38, 122]. Incorporating this effect into a mesoscale elastic model of dissociated dislocations would enable to investigate the interplay between this additional contribution and the solute/partial dislocation interaction in a consistent framework.

Acknowledgment

The author acknowledge the support of the French Agence Nationale de la Recherche (ANR), under grant ANR-20-CE08-0019 (project INSPIRA).The author would like to warmly thank David Rodney and Céline Varvenne for fruitful discussion on this topic.

References

[1] A. Argon, Strengthening mechanisms in crystal plasticity, volume 4, OUP Oxford, 2007.
[2] D. Hull, D. J. Bacon, Introduction to dislocations, volume 37, Elsevier, 2011.
[3] J. R. Davis, et al., Aluminum and aluminum alloys, ASM international, 1993.
[4] P. Marshall, Austenitic stainless steels: microstructure and mechanical properties, Springer Science & Business Media, 1984.
[5] H. Long, S. Mao, Y. Liu, Z. Zhang, X. Han, Microstructural and compositional design of Ni-based single crystalline superalloys—a review, Journal of Alloys and Compounds 743 (2018) 203–220. doi:10.1016/j.jallcom.2018.01.224.
[6] E. Akca, A. Gürsel, A review on superalloys and IN718 nickel-based Inconel superalloy, Periodicals of engineering and natural sciences 3 (2015). doi:10.21533/pen.v3i1.43.

[7] Z. Wu, H. Bei, G. M. Pharr, E. P. George, Temperature dependence of the mechanical properties of equiatomic solid solution alloys with face-centered cubic crystal structures, Acta Materialia 81 (2014) 428–441. doi:10.1016/j.actamat.2014.08.026.

[8] M.-H. Tsai, J.-W. Yeh, High-entropy alloys: a critical review, Materials Research Letters 2 (2014) 107–123. doi:10.1080/21663831.2014.912690.

[9] O. N. Senkov, D. B. Miracle, K. J. Chaput, J.-P. Couzinie, Development and exploration of refractory high entropy alloys—a review, Journal of Materials Research 33 (2018) 3092–3128. doi:10.1557/jmr.2018.153.

[10] E. P. George, W. Curtin, C. C. Tasan, High entropy alloys: A focused review of mechanical properties and deformation mechanisms, Acta Materialia 188 (2020) 435–474. doi:10.1016/j.actamat.2019.12.015.

[11] B. Cantor, Multicomponent high-entropy Cantor alloys, Progress in Materials Science 120 (2021) 100754. doi:10.1016/j.pmatsci.2020.100754.

[12] H. Suzuki, Solid solution hardening in body-centred cubic alloys, Dislocations in solids 4 (1980) 191–217.

[13] C. Varvenne, G. P. M. Leyson, M. Ghazisaeidi, W. A. Curtin, Solute strengthening in random alloys, Acta Materialia 124 (2017) 660–683. doi:10.1016/j.actamat.2016.09.046.

[14] I. Baker, Interstitial strengthening in FCC metals and alloys, Advanced Powder Materials 1 (2022) 100034. doi:10.1016/j.apmate.2022.100034.

[15] J. Hirth, J. Lothe, Theory of Dislocations, McGraw-Hill, New York, 1968.

[16] W. A. Curtin, D. L. Olmsted, L. G. Hector Jr, A predictive mechanism for dynamic strain ageing in aluminium–magnesium alloys, Nature materials 5 (2006) 875–880. doi:10.1038/nmat1765.

[17] R. Bullough, R. Newman, The kinetics of migration of point defects to dislocations, Reports on progress in physics 33 (1970) 101. doi:10.1088/0034-4885/33/1/303.

[18] J. D. Eshelby, The determination of the elastic field of an ellipsoidal inclusion, and related problems, Proceedings of the royal society of London. Series A. Mathematical and physical sciences 241 (1957) 376–396. doi:10.1098/rspa.1957.0133.

[19] H. Suzuki, The yield strength of binary alloys, Dislocations and mechanical properties of crystals (1957) 361–390.

[20] H. Suzuki, Segregation of solute atoms to stacking faults, Journal of the Physical Society of Japan 17 (1962) 322–325. doi:10.1143/JPSJ.17.322.

[21] E. Rodary, D. Rodney, L. Proville, Y. Bréchet, G. Martin, Dislocation glide in model Ni(Al) solid solutions by molecular dynamics, Physical Review B 70 (2004) 054111. doi:10.1103/PhysRevB.70.054111.

[22] L. Proville, D. Rodney, Y. Brechet, G. Martin, Atomic-scale study of dislocation glide in a model solid solution, Philosophical Magazine 86 (2006) 3893–3920. doi:10.1080/14786430600567721.

[23] D. Bacon, Y. N. Osetsky, D. Rodney, Dislocation–obstacle interactions at the atomic level, Dislocations in solids 15 (2009) 1–90. doi:10.1016/S1572-4859(09)01501-0.

[24] R. Labusch, A statistical theory of solid solution hardening, Physica Status Solidi (b) 41 (1970) 659–669. doi:10.1002/pssb.19700410221.

[25] G. P. M. Leyson, W. A. Curtin, L. G. Hector, C. F. Woodward, Quantitative prediction of solute strengthening in aluminium alloys, Nature Materials 9 (2010) 750–755. doi:10.1038/nmat2813.

[26] C. Varvenne, A. Luque, W. A. Curtin, Theory of strengthening in FCC high entropy alloys, Acta Materialia 118 (2016) 164–176. doi:10.1016/j.actamat.2016.07.040.

[27] D. L. Olmsted, L. G. Hector, W. Curtin, R. Clifton, Atomistic simulations of dislocation mobility in Al, Ni and Al/Mg alloys, Modelling and Simulation in Materials Science and Engineering 13 (2005) 371. doi:10.1088/0965-0393/13/3/007.

[28] S. Patinet, L. Proville, Dislocation pinning by substitutional impurities in an atomic-scale model for al(mg) solid solutions, Philosophical Magazine 91 (2011) 1581–1606. doi:10.1080/14786435.2010.543649.

[29] J. Marian, A. Caro, Moving dislocations in disordered alloys: Connecting continuum and discrete models with atomistic simulations, Physical Review B 74 (2006) 024113. doi:10.1103/PhysRevB.74.024113.

[30] S. Patinet, L. Proville, Depinning transition for a screw dislocation in a model solid solution, Physical Review B 78 (2008) 104109. doi:10.1103/PhysRevB.78.104109.

[31] S. I. Rao, C. Woodward, T. A. Parthasarathy, O. Senkov, Atomistic simulations of dislocation behavior in a model FCC multicomponent concentrated solid solution alloy, Acta Materialia 134 (2017) 188–194. doi:10.1016/j.actamat.2017.05.071.

[32] W. Li, S. I. Rao, Q. Wang, H. Fan, J. Yang, J. A. El-Awady, Core structure and mobility of edge dislocations in face-centered-cubic chemically complex NiCoFe and NiCoFeCu equiatomic solid-solution alloys, Materialia 9 (2020) 100628. doi:10.1016/j.mtla.2020.100628.

[33] A. Daramola, A. Fraczkiewicz, G. Bonny, A. Nomoto, G. Adjanor, C. Domain, G. Monnet, Atomistic investigation of elementary dislocation properties influencing mechanical behaviour of $Cr_{15}Fe_{46}Mn_{17}Ni_{22}$ alloy and $Cr_{20}Fe_{70}Ni_{10}$ alloy, Computational Materials Science 211 (2022) 111508. doi:10.1016/j.commatsci.2022.111508.

[34] R. B. Sills, M. E. Foster, X. W. Zhou, Line-length-dependent dislocation mobilities in an FCC stainless steel alloy, International Journal of Plasticity 135 (2020) 102791. doi:10.1016/j.ijplas.2020.102791.

[35] T. M. Smith, M. S. Hooshmand, B. D. Esser, F. Otto, D. W. McComb, E. P. George, M. Ghazisaeidi, M. J. Mills, Atomic-scale characterization and modeling of 60 dislocations in a high-entropy alloy, Acta Materialia 110 (2016) 352–363. doi:10.1016/j.actamat.2016.03.045.

[36] C. Baruffi, M. Ghazisaeidi, D. Rodney, W. Curtin, Equilibrium versus non-equilibrium stacking fault widths in NiCoCr, Scripta Materialia 235 (2023) 115536. doi:10.1016/j.scriptamat.2023.115536.

[37] M. Shih, J. Miao, M. Mills, M. Ghazisaeidi, Stacking fault energy in concentrated alloys, Nature communications 12 (2021) 3590. doi:10.1038/s41467-021-23860-z.

[38] A. Esfandiarpour, S. Papanikolaou, M. Alava, Edge dislocations in multicomponent solid solution alloys: Beyond traditional elastic depinning, Physical Review Research 4 (2022) L022043. doi:10.1103/PhysRevResearch.4.L022043.

[39] R. Pasianot, D. Farkas, Atomistic modeling of dislocations in a random quinary high-entropy alloy, Computational Materials Science 173 (2020) 109366. doi:10.1016/j.commatsci.2019.109366.

[40] G. Péterffy, P. D. Ispánovity, M. E. Foster, X. Zhou, R. B. Sills, Length scales and scale-free dynamics of dislocations in dense solid solutions, Materials Theory 4 (2020) 1–25. doi:10.1186/s41313-020-00023-z.

[41] S. Patinet, D. Bonamy, L. Proville, Atomic-scale avalanche along a dislocation in a random alloy, Physical Review B 84 (2011) 174101. doi:10.1103/PhysRevB.84.174101.

[42] E. Antillon, C. Woodward, S. Rao, B. Akdim, T. Parthasarathy,

Chemical short range order strengthening in a model FCC high entropy alloy, Acta Materialia 190 (2020) 29–42. doi:10.1016/j.actamat.2020.02.041.

[43] A. Abu-Odeh, D. L. Olmsted, M. Asta, Screw dislocation mobility in a face-centered cubic solid solution with short-range order, Scripta Materialia 210 (2022) 114465. doi:10.1016/j.scriptamat.2021.114465.

[44] S. Chen, Z. H. Aitken, S. Pattamatta, Z. Wu, Z. G. Yu, D. J. Srolovitz, P. K. Liaw, Y.-W. Zhang, Simultaneously enhancing the ultimate strength and ductility of high-entropy alloys via short-range ordering, Nature communications 12 (2021) 4953. doi:10.1038/s41467-021-25264-5.

[45] L. Proville, S. Patinet, Atomic-scale models for hardening in FCC solid solutions, Physical Review B 82 (2010) 054115. doi:10.1103/PhysRevB.82.054115.

[46] L. A. Zepeda-Ruiz, A. Stukowski, T. Oppelstrup, V. V. Bulatov, Probing the limits of metal plasticity with molecular dynamics simulations, Nature 550 (2017) 492–495. doi:10.1038/nature23472.

[47] M. S. Daw, S. M. Foiles, M. I. Baskes, The embedded-atom method: a review of theory and applications, Materials Science Reports 9 (1993) 251–310. doi:10.1016/0920-2307(93)90001-U.

[48] X. Zhou, R. Johnson, H. Wadley, Misfit-energy-increasing dislocations in vapor-deposited CoFe/NiFe multilayers, Physical Review B 69 (2004) 144113. doi:10.1103/PhysRevB.69.144113.

[49] F. Wang, H.-H. Wu, L. Dong, G. Pan, X. Zhou, S. Wang, R. Guo, G. Wu, J. Gao, F.-Z. Dai, et al., Atomic-scale simulations in multi-component alloys and compounds: A review on advances in interatomic potential, Journal of Materials Science & Technology (2023). doi:10.1016/j.jmst.2023.05.010.

[50] Y. Zuo, C. Chen, X. Li, Z. Deng, Y. Chen, J. Behler, G. Csányi, A. V. Shapeev, A. P. Thompson, M. A. Wood, et al., Performance and cost assessment of machine learning interatomic potentials, The Journal of Physical Chemistry A 124 (2020) 731–745. doi:10.1021/acs.jpca.9b08723.

[51] G. L. Hart, T. Mueller, C. Toher, S. Curtarolo, Machine learning for alloys, Nature Reviews Materials 6 (2021) 730–755. doi:10.1038/s41578-021-00340-w.

[52] Y. Mishin, Machine-learning interatomic potentials for materials science, Acta Materialia 214 (2021) 116980. doi:10.1016/j.actamat.2021.116980.

[53] S. Starikov, D. Smirnova, T. Pradhan, Y. Lysogorskiy, H. Chapman, M. Mrovec, R. Drautz, Angular-dependent interatomic potential for large-scale atomistic simulation of iron: Development and comprehensive comparison with existing interatomic models, Physical Review Materials 5 (2021) 063607. doi:10.1103/PhysRevMaterials.5.063607.

[54] M. Benoit, J. Amodeo, S. Combettes, I. Khaled, A. Roux, J. Lam, Measuring transferability issues in machine-learning force fields: the example of gold–iron interactions with linearized potentials, Machine Learning: Science and Technology 2 (2020) 025003. doi:10.1088/2632-2153/abc9fd.

[55] R. Fleischer, Solution hardening, Acta Metallurgica 9 (1961) 996–1000. doi:10.1016/0001-6160(61)90242-5.

[56] U. Kocks, Statistical treatment of penetrable obstacles, Canadian Journal of Physics 45 (1967) 737–755. doi:10.1139/p67-056.

[57] N. Mott, F. Nabarro, Report of a conference on the strength of solids, Bristol, 1948.

[58] F. Nabarro, The theory of solution hardening, Philosophical Magazine 35 (1977) 613–622. doi:10.1080/14786437708235994.

[59] R. Labusch, Statistische theorien der mischkristallhärtung, Acta metallurgica 20 (1972) 917–927. doi:10.1016/0001-6160(72)90085-5.

[60] J. Friedel, Dislocations: International Series of Monographs on Solid State Physics, volume 3, Elsevier, 2013.

[61] G. Leyson, W. Curtin, Friedel vs. labusch: the strong/weak pinning transition in solute strengthened metals, Philosophical Magazine 93 (2013) 2428–2444. doi:10.1080/14786435.2013.776718.

[62] N. Mott, CXVII. a theory of work-hardening of metal crystals, The London, Edinburgh, and Dublin Philosophical Magazine and Journal of Science 43 (1952) 1151–1178. doi:10.1080/14786441108521024.

[63] M. Zaiser, Dislocation motion in a random solid solution, Philosophical Magazine A 82 (2002) 2869–2883. doi:10.1080/01418610208240071.

[64] I. Toda-Caraballo, P. E. Rivera-Díaz-del Castillo, Modelling solid solution hardening in high entropy alloys, Acta Materialia 85 (2015) 14–23. doi:10.1016/j.actamat.2014.11.014.

[65] M. Walbrühl, D. Linder, J. Ågren, A. Borgenstam, Modelling of solid solution strengthening in multicomponent alloys, Materials Science and Engineering: A 700 (2017) 301–311. doi:10.1016/j.msea.2017.06.001.

[66] S. Nag, W. A. Curtin, Effect of solute-solute interactions on strengthening of random alloys from dilute to high entropy alloys, Acta Materialia 200 (2020) 659–673. doi:10.1016/j.actamat.2020.08.011.

[67] B. Yin, L. Li, S. Drescher, S. Seils, S. Nag, J. Freudenberger, W. Curtin, Solute misfit and solute interaction effects on strengthening: A case study in AuNi, Acta Materialia (2023) 119118. doi:10.1016/j.actamat.2023.119118.

[68] D. L. Olmsted, L. G. Hector Jr, W. Curtin, Molecular dynamics study of solute strengthening in Al/Mg alloys, Journal of the Mechanics and Physics of Solids 54 (2006) 1763–1788. doi:10.1016/j.jmps.2005.12.008.

[69] B. Szajewski, F. Pavia, W. Curtin, Robust atomistic calculation of dislocation line tension, Modelling and Simulation in Materials Science and Engineering 23 (2015) 085008. doi:10.1088/0965-0393/23/8/085008.

[70] Y. Hu, B. Szajewski, D. Rodney, W. Curtin, Atomistic dislocation core energies and calibration of non-singular discrete dislocation dynamics, Modelling and Simulation in Materials Science and Engineering 28 (2019) 015005. doi:10.1088/1361-651X/ab5489.

[71] P.-A. Geslin, D. Rodney, Thermal fluctuations of dislocations reveal the interplay between their core energy and long-range elasticity, Physical Review B 98 (2018) 174115. doi:10.1103/PhysRevB.98.174115.

[72] P.-A. Geslin, D. Rodney, Investigation of partial dislocations fluctuations yields dislocation core parameters, Modelling and Simulation in Materials Science and Engineering 28 (2020) 055006. doi:10.1088/1361-651X/ab8a96.

[73] G. P. M. Leyson, L. Hector Jr, W. A. Curtin, Solute strengthening from first principles and application to aluminum alloys, Acta Materialia 60 (2012) 3873–3884. doi:10.1016/j.actamat.2012.03.037.

[74] D. Ma, M. Friák, J. von Pezold, D. Raabe, J. Neugebauer, Computationally efficient and quantitatively accurate multiscale simulation of solid-solution strengthening by ab initio calculation, Acta Materialia 85 (2015) 53–66. doi:10.1016/j.actamat.2014.10.044.

[75] G. Schoeck, The peierls model: progress and limitations, Materials Science and Engineering: A 400 (2005) 7–17. doi:10.1016/j.msea.2005.03.050.

[76] C. Varvenne, A. Luque, W. G. Nöhring, W. A. Curtin, Average-

atom interatomic potential for random alloys, Physical Review B 93 (2016) 104201. doi:10.1103/PhysRevB.93.104201.
[77] A. Zunger, S.-H. Wei, L. Ferreira, J. E. Bernard, Special quasirandom structures, Physical review letters 65 (1990) 353. doi:10.1103/PhysRevLett.65.353.
[78] A. Zaddach, C. Niu, C. Koch, D. Irving, Mechanical properties and stacking fault energies of NiFeCrCoMn high-entropy alloy, Jom 65 (2013) 1780–1789. doi:10.1007/s11837-013-0771-4.
[79] Y. Ikeda, B. Grabowski, F. Körmann, Ab initio phase stabilities and mechanical properties of multicomponent alloys: A comprehensive review for high entropy alloys and compositionally complex alloys, Materials Characterization 147 (2019) 464–511. doi:10.1016/j.matchar.2018.06.019.
[80] B. Yin, W. A. Curtin, First-principles-based prediction of yield strength in the RhIrPdPtNiCu high-entropy alloy, npj Computational Materials 5 (2019) 14. doi:10.1038/s41524-019-0151-x.
[81] B. Yin, S. Yoshida, N. Tsuji, W. Curtin, Yield strength and misfit volumes of NiCoCr and implications for short-range-order, Nature communications 11 (2020) 2507. doi:10.1038/s41467-020-16083-1.
[82] M. Laurent-Brocq, L. Perrière, R. Pirès, F. Prima, P. Vermaut, Y. Champion, From diluted solid solutions to high entropy alloys: On the evolution of properties with composition of multi-components alloys, Materials Science and Engineering: A 696 (2017) 228–235. doi:10.1016/j.msea.2017.04.079.
[83] F. G. Coury, K. D. Clarke, C. S. Kiminami, M. J. Kaufman, A. J. Clarke, High throughput discovery and design of strong multicomponent metallic solid solutions, Scientific reports 8 (2018) 8600. doi:10.1038/s41598-018-26830-6.
[84] C. Varvenne, W. A. Curtin, Strengthening of high entropy alloys by dilute solute additions: $CoCrFeNiAl_x$ and $CoCrFeNiMnAl_x$ alloys, Scripta Materialia 138 (2017) 92–95. doi:10.1016/j.scriptamat.2017.05.035.
[85] B. Yin, W. Curtin, Origin of high strength in the CoCrFeNiPd high-entropy alloy, Materials Research Letters 8 (2020) 209–215. doi:10.1080/21663831.2020.1739156.
[86] B. Yin, F. Maresca, W. Curtin, Vanadium is an optimal element for strengthening in both FCC and BCC high-entropy alloys, Acta Materialia 188 (2020) 486–491. doi:10.1016/j.actamat.2020.01.062.
[87] C. Varvenne, W. A. Curtin, Predicting yield strengths of noble metal high entropy alloys, Scripta Materialia 142 (2018) 92–95. doi:10.1016/j.scriptamat.2017.08.030.
[88] F. Thiel, D. Utt, A. Kauffmann, K. Nielsch, K. Albe, M. Heilmaier, J. Freudenberger, Breakdown of Varvenne scaling in $(AuNiPdPt)_{1-x}cu_x$ high-entropy alloys, Scripta Materialia 181 (2020) 15–18. doi:10.1016/j.scriptamat.2020.02.007.
[89] J. Freudenberger, F. Thiel, D. Utt, K. Albe, A. Kauffmann, S. Seils, M. Heilmaier, Solid solution strengthening in medium-to high-entropy alloys, Materials Science and Engineering: A 861 (2022) 144271. doi:10.1016/j.msea.2022.144271.
[90] C. Wen, C. Wang, Y. Zhang, S. Antonov, D. Xue, T. Lookman, Y. Su, Modeling solid solution strengthening in high entropy alloys using machine learning, Acta Materialia 212 (2021) 116917. doi:10.1016/j.actamat.2021.116917.
[91] X. Huang, C. Jin, C. Zhang, H. Zhang, H. Fu, Machine learning assisted modelling and design of solid solution hardened high entropy alloys, Materials & Design 211 (2021) 110177. doi:10.1016/j.matdes.2021.110177.
[92] A. Foreman, M. Makin, Dislocation movement through random arrays of obstacles, Philosophical magazine 14 (1966) 911–924. doi:10.1080/14786436608244762.
[93] R. Arsenault, S. Patu, D. Esterling, Computer simulation of solid solution strengthening in FCC alloys: Part I. Friedel and Mott limits, Metallurgical Transactions A 20 (1989) 1411–1418. doi:10.1007/BF02665498.
[94] R. Arsenault, S. Patu, D. Esterling, Computer simulation of solid solution strengthening in FCC alloys: Part II. At absolute zero temperature, Metallurgical Transactions A 20 (1989) 1419–1428. doi:10.1007/BF02665499.
[95] L. Proville, Depinning of a discrete elastic string from a random array of weak pinning points with finite dimensions, Journal of Statistical Physics 137 (2009) 717–727. doi:10.1007/s10955-009-9860-8.
[96] J.-H. Zhai, M. Zaiser, Properties of dislocation lines in crystals with strong atomic-scale disorder, Materials Science and Engineering: A 740 (2019) 285–294. doi:10.1016/j.msea.2018.10.010.
[97] P.-A. Geslin, D. Rodney, Microelasticity model of random alloys. Part I: mean square displacements and stresses, Journal of the Mechanics and Physics of Solids 153 (2021) 104479. doi:10.1016/j.jmps.2021.104479.
[98] P.-A. Geslin, A. Rida, D. Rodney, Microelasticity model of random alloys. Part II: displacement and stress correlations, Journal of the Mechanics and Physics of Solids 153 (2021) 104480. doi:10.1016/j.jmps.2021.104480.
[99] A. Lemaître, Stress correlations in glasses, The Journal of Chemical Physics 149 (2018) 104107. doi:10.1063/1.5041461.
[100] A. Rida, E. Martinez, D. Rodney, P.-A. Geslin, Influence of stress correlations on dislocation glide in random alloys, Physical Review Materials 6 (2022) 033605. doi:10.1103/PhysRevMaterials.6.033605.
[101] A. Larkin, Y. Ovchinnikov, Pinning in type II superconductors, Journal of Low Temperature Physics 34 (1979) 409–428. doi:10.1007/BF00117160.
[102] A.-L. Barabási, H. E. Stanley, et al., Fractal concepts in surface growth, Cambridge university press, 1995.
[103] S. Zapperi, M. Zaiser, Depinning of a dislocation: the influence of long-range interactions, Materials Science and Engineering: A 309 (2001) 348–351. doi:10.1016/S0921-5093(00)01627-0.
[104] M. Zaiser, R. Wu, Pinning of dislocations in disordered alloys: effects of dislocation orientation, Materials Theory 6 (2022) 4. doi:10.1186/s41313-021-00036-2.
[105] A. Vaid, E. Bitzek, S. Nasiri, M. Zaiser, et al., Pinning of extended dislocations in atomically disordered crystals, Acta Materialia 236 (2022) 118095. doi:10.1016/j.actamat.2022.118095.
[106] R. Labusch, G. Grange, J. Ahearn, P. Haasen, Rate processes in plastic deformation of materials, in: Proceedings from John E. Dorn Symposium, edited by J.C.M. Li and A.K. Mukherjee, American Society for Metals, Metal Park, Ohio, 1975, p. 26.
[107] M. E. Kassner, Fundamentals of creep in metals and alloys, Butterworth-Heinemann, 2015.
[108] Z. Basinski, R. Foxall, R. Pascual, Stress equivalence of solution hardening, Scripta Metallurgica 6 (1972) 807–814. doi:10.1016/0036-9748(72)90052-X.
[109] G. Laplanche, J. Bonneville, C. Varvenne, W. Curtin, E. P. George, Thermal activation parameters of plastic flow reveal deformation mechanisms in the crmnfeconi high-entropy alloy, Acta Materialia 143 (2018) 257–264. doi:10.1016/j.actamat.2017.10.014.
[110] G. Leyson, W. Curtin, Solute strengthening at high temperatures, Modelling and Simulation in Materials Science and Engineering 24 (2016) 065005. doi:10.1088/0965-0393/24/6/065005.

[111] V. M. Vinokur, M. C. Marchetti, L.-W. Chen, Glassy motion of elastic manifolds, Physical review letters 77 (1996) 1845. doi:10.1103/PhysRevLett.77.1845.

[112] E. E. Ferrero, S. Bustingorry, A. B. Kolton, A. Rosso, Numerical approaches on driven elastic interfaces in random media, Comptes Rendus Physique 14 (2013) 641–650. doi:10.1016/j.crhy.2013.08.002.

[113] E. E. Ferrero, L. Foini, T. Giamarchi, A. B. Kolton, A. Rosso, Creep motion of elastic interfaces driven in a disordered landscape, Annual Review of Condensed Matter Physics 12 (2021) 111–134. doi:10.1146/annurev-conmatphys-031119-050725.

[114] T. Nattermann, Scaling approach to pinning: Charge density waves and giant flux creep in superconductors, Physical review letters 64 (1990) 2454. doi:10.1103/PhysRevLett.64.2454.

[115] A. B. Kolton, A. Rosso, T. Giamarchi, Creep motion of an elastic string in a random potential, Physical review letters 94 (2005) 047002. doi:10.1103/PhysRevLett.64.2454.

[116] A. B. Kolton, A. Rosso, T. Giamarchi, W. Krauth, Creep dynamics of elastic manifolds via exact transition pathways, Physical Review B 79 (2009) 184207. doi:10.1103/PhysRevB.79.184207.

[117] E. E. Ferrero, L. Foini, T. Giamarchi, A. B. Kolton, A. Rosso, Spatiotemporal patterns in ultraslow domain wall creep dynamics, Physical review letters 118 (2017) 147208. doi:10.1103/PhysRevLett.118.147208.

[118] C. Sobie, L. Capolungo, D. L. McDowell, E. Martinez, Thermal activation of dislocations in large scale obstacle bypass, Journal of the Mechanics and Physics of Solids 105 (2017) 150–160. doi:10.1016/j.jmps.2017.05.003.

[119] C. Sobie, L. Capolungo, D. L. McDowell, E. Martinez, Scale transition using dislocation dynamics and the nudged elastic band method, Journal of the Mechanics and Physics of Solids 105 (2017) 161–178. doi:10.1016/j.jmps.2017.05.004.

[120] P.-A. Geslin, R. Gatti, B. Devincre, D. Rodney, Implementation of the nudged elastic band method in a dislocation dynamics formalism: Application to dislocation nucleation, Journal of the Mechanics and Physics of Solids 108 (2017) 49–67. doi:10.1016/j.jmps.2017.07.019.

[121] B. Sboui, D. Rodney, P.-A. Geslin, Elastic modelling of lattice distortions in concentrated random alloys, Acta Materialia 257 (2023) 119117. doi:10.1016/j.actamat.2023.119117.

[122] Y. Zeng, X. Cai, M. Koslowski, Effects of the stacking fault energy fluctuations on the strengthening of alloys, Acta Materialia 164 (2019) 1–11. doi:10.1016/j.actamat.2018.09.066.